CHEMISTRY & CHEMICAL TECHNOLOGY

Chem. Chem. Technol., 2026,
Vol. 20, No. 1, pp. 001–009

Chemistry

MECHANICAL AND MICROSTRUCTURAL CHARACTERIZATION OF AN AlCuAg ALLOY

Ángel A. Coutiño-Martínez[1], José Amparo Rodríguez-García[1], Carlos Adrián Calles-Arriaga[1], José A. Castillo-Robles[1], Wilian Jesús Pech-Rodríguez[1], José Guadalupe Miranda-Hernández[2] and Enrique Rocha-Rangel[1,✉]

[1] Universidad Politécnica de Victoria, Av. Nuevas Tecnologías, 5902, Ciudad Victoria, Tamaulipas, 87138, México
[2] Centro Universitario UAEM Valle de México, Atizapán de Zaragoza, Estado de México, 54500, México
✉ *erochar@upv.edu.mx*

https://doi.org/10.23939/chcht20.01.001

Abstract. Aluminum alloys are widely used in the automotive and aeronautical industries due to their good mechanical properties, high corrosion resistance, and low weight. In this study, an aluminum-based medium-entropy alloy was fabricated by adding copper and silver. The alloy composition consisted of 97 wt. % aluminum, with 1.5 wt. % copper and 1.5 wt. % silver. The processing technique was carried out using the powder metallurgical route. After the sintering phase, different thermal aging treatments were conducted to improve the aluminum alloy's mechanical properties. Heat treatments were performed at different times and temperatures. The results revealed a microstructure with very fine grain sizes, consisting of two phases: an α-solid solution matrix with a composition close to the nominal alloy, and an intermetallic β-phase composed of dispersed, copper-rich AlCuAg precipitates.

Keywords: alloys, multicomponent, medium entropy alloys, AlCuAg.

1. Introduction

Aluminum is the most abundant metallic material on Earth. In its pure state, it is soft, but when combined with other metals, its mechanical properties are considerably improved. It exhibits good electrical and thermal conductivity and is very ductile, malleable, and corrosion-resistant. The most attractive features of aluminum are its low density, low cost, and its ability to be heat-treated to increase its strength.[1, 2] For these reasons, aluminum alloys are widely used in the aerospace and automotive industries. Recently, new alloys have been developed to enhance strength and stiffness for the next generation of aircraft and vehicles. To this end, several studies have incorporated rare earth elements into aluminum alloys to improve tensile strength, heat resistance, and corrosion resistance.[3, 4]

On the other hand, the conventional method of designing alloys for many years has been to start with a base element and add small portions of other metals to enhance their properties, thus forming families of alloys such as steel, which has iron as its main element. This approach has resulted in extensive knowledge about materials derived from a base component.[5, 6] However, in recent years, the exploration of alloys composed of multiple elements in varying proportions has led to the emergence of multicomponent alloys.[6–12] These alloys can be conceptually classified based on their configurational entropy (ΔS).[11] If ΔS exceeds 1.5 R (where R is the gas constant), the alloy is considered a high-entropy alloy (HEA). Conversely, if ΔS is between 1.0 R and 1.5 R, it is classified as a medium-entropy alloy (MEA). However, medium and high entropy alloys (M/HEAs) can be simply defined as simple solid-solution alloys composed of three or more principal elements.[14, 15] HEA have been studied recently due to their high entropy effects. However, it has been found that a high number of components are not necessarily required to achieve these effects, but that this can be achieved with only a few main elements. Thus, giving rise to medium-entropy alloys; these proportions need not be in the strict sense of the definition, equiatomic either.[16] In other words, some non-equiatomic alloys have been shown to exhibit superior mechanical properties compared to their equiatomic counterparts. This further increases the number of compositions that can be carried out to develop new alloys. Unlike HEA, MEA has a

configuration that allows it to maintain a balance between the simplicity of its structure and the complex properties derived from the interaction of its components.[17] Due to the high grain boundaries and dislocations, these alloys can exhibit high strength and hardness while maintaining good ductility and toughness. Several studies have shown that a balance between mechanical properties and wear resistance can be achieved by retaining a simple structure, which provides structural stability, such as body-centered cubic (BCC), as observed in the non-equiatomic Ni-Co-Fe system with Al additions.[18] Other systems show microstructural characteristics with 2 ordered face-centered cubic (FCC) and BCC phases with nanoprecipitates uniformly distributed within the matrix, as in the medium entropy Al-Co-Cr-Ni alloy exhibiting excellent compressive properties and fracture toughness exceeding 2000 MPa.[19] Theoretical and experimental studies on crystal structure properties have primarily focused on alloys located near the corners and edges of ternary multi-component phase diagrams, resulting in a well-established understanding of these regions. However, this level of insight does not extend to systems whose alloys are situated near the center of the diagram. Because there are no phase diagrams in quaternary and higher systems, most of the solid solutions in HEA are identified by trial-and-error experiments.[20] This has led to the study of ternary alloys with compositions close to one of the corners of the corresponding phase diagram. Thus, this work aims to fabricate a medium-entropy alloy in the aluminum-rich region with small additions of copper and silver and to characterize the alloy both mechanically and microstructurally after it has been subjected to different aging heat treatments.

2. Experimental

2.1. Materials and methods

Elemental powders of Al, Cu, and Ag with a purity greater than 99 % and sizes of ~5 μm, in 97, 1.5, and 1.5 wt. % proportions, respectively, were mechanically processed in a high-energy planetary mill (Retsch, PM 100, Germany). The grinding parameters used in the mixture were as follows: dry grinding for 6 hours at 300 rpm, using isopropyl alcohol as a control agent, and maintaining a ball weight to powder weight ratio of 10:1. Once the powders were ground, they were pressed to form cylindrical pellets with an average diameter and height of 10 mm and 3 mm respectively, using a tool grade steel die. Compaction of these samples was carried out at room temperature by uniaxial pressing using a pressure of 300 kg/cm^2 in a hydraulic press (Montequipo, LAB-30T, Mexico). Afterward, all the pellets were sintered in an electric furnace (Carbolite RHF 17/3E, England) at 600 °C for 2 h, with a heating rate of 10 °C/min. The furnace was set up with a protective argon atmosphere to prevent oxidation of the metals. The work focused on studying the effect of thermal aging treatments on the mechanical properties of sintered alloy. For this purpose, four treatments were carried out to explore which one offers the best mechanical characteristics. These treatments are described in Table 1. After the grinding stage, the particle size distribution and specific surface area were determined using a Mastersizer 2000 instrument (England). Before characterizing the sintered samples, they were ground using SiC sandpaper and then polished with alumina and diamond suspensions. The crystalline phases present in the sintered alloys were identified by X-ray diffraction (XRD) analysis using CuKα radiation. The measurements were performed on an X'Pert PRO diffractometer (PANalytical) and analyzed using the X'Pert Highscore Plus PANalytical software using patterns in the ICDD PDF2 database. Additionally, the microstructure of the alloys was examined using scanning electron microscopy (SEM) and an energy-dispersive spectrometer (EDS) detector on a Hitachi SU3500 microscope. The microstructure after annealing treatments was analyzed using optical microscopy (Nikon 2000 plus, Japan). Finally, the study samples were characterized in order to determine their mechanical properties. The mechanical properties evaluated in this study included microhardness and compressive strength. Microhardness measurements were conducted in accordance with the ASTM E384–16 standard.[21] A total of twelve measurements were made at different locations on each sample, and the average value is reported. These measurements were performed using a microhardness tester (Wilson Instruments Model S400, USA). Compressive strength testing was carried out using a universal material tester (WP 300 GUNT, Germany), from which the elastic modulus, yield stress, maximum stress, and fracture stress of the alloy were determined. The tester machine is equipped with a 20 kN load cell. For the test, a head displacement rate of 10 mm/min in 2 cm diameter cylindrical samples was used. The fracture stress is determined at the moment the sample fractures.

Table 1. Aging hardening heat treatments

Sample	Heating rate, ºC/min	Temperature, ºC	Holding, h
Sample 1	10	350	5
Sample 2	10	350	2
Sample 3	10	300	5
Sample 4	10	300	2

3. Results and Discussion

3.1. Particle size

Fig. 1 shows the particle size distribution and the accumulated particle size obtained after the mechanical milling process. The milling effectively reduced the initial particle sizes, which exceeded 4–5 microns, yielding particles within the range of 2.3 to 3.4 μm with an average of 2.8 μm. However, there may be some smaller particles that the equipment could not detect. Finer particles can lead to a more homogeneous distribution in the composite material, which in turn affects the efficiency of downstream processes such as compaction or sintering. Using the software associated with the laser diffraction equipment, the following particle size values were obtained: an average particle size of 2.82 μm, a median of 2.78 μm, and a mode of 2.73 μm, with a standard deviation of 0.043 μm.

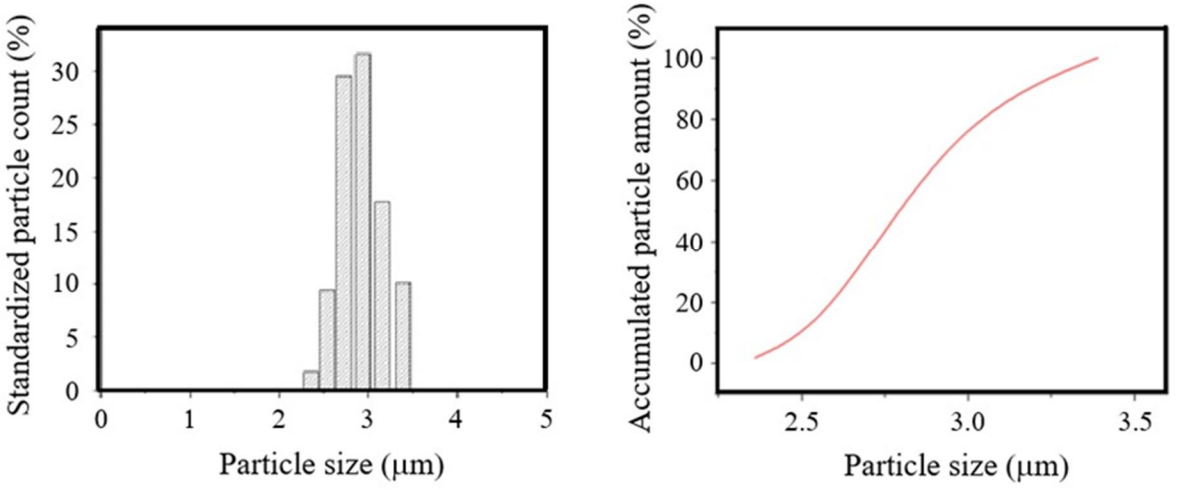

Fig. 1. Normal and cumulative particle size distribution of AlCuAg alloy powders

3.2. Structure

The alloy powders were analyzed by X-ray diffraction after 6 h of milling. The obtained diffractogram, shown in Fig. 2, was analyzed using the X'Pert HighScore Plus program, and a 99 % correspondence was found with the crystallographic table 01-085-1327. The AlCuAg powders exhibit a cubic crystalline system; however, the study revealed only the most important peaks characteristic of Al. The Cu and Ag peaks were not observed because the equipment could not detect them at compositions below 2 %. The diffractogram shows the X-ray diffraction patterns of aluminum with the most intense peaks at 2 theta angles of 38.4 and 44.7, corresponding to the (111) and (002) planes, respectively. Likewise, the alloy exhibits a face-centered cubic (FCC) crystal structure, as all three elements share this structure.

The lattice constant of the synthesized alloy was calculated using Bragg's law equation, based on the interplanar distance (dhkl), using the peaks at $2\theta = 38.4°$ corresponding to the (111) planes of the FCC structure. By knowing the value of dhkl and using Equation (1), which relates the interplanar distance to the lattice parameter in cubic systems, the latter was determined. The lattice parameter value determined for the alloy was 4.04 Å, which, compared to the value of 4.05 Å reported in the literature for pure aluminum,[2] is slightly lower.

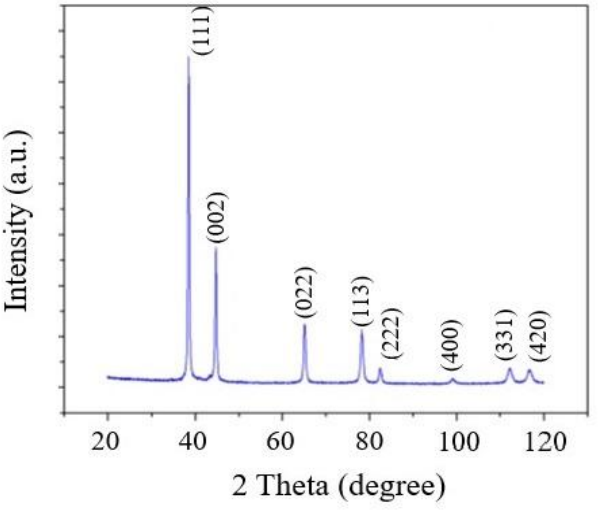

Fig. 2. Diffraction pattern corresponding to the AlCuAg alloy

This slight discrepancy in the lattice parameter of aluminum is due to the presence of copper, whose lattice parameter (3.61 Å) is smaller than that of aluminum and

silver (4.09 Å). The smaller lattice parameter observed for copper is attributable to its smaller atomic radius compared to that of aluminum and silver. Consequently, copper atoms can substitute for some aluminum atoms within the crystal lattice, leading to structural distortion. This distortion is expected to influence the mechanical properties of the alloy.

$$a = d_{hkl}\sqrt{h^2 + k^2 + l^2}. \quad (1)$$

3.3. Microstructure

Fig. 3 shows the alloy's microstructure observed by optical microscopy at 200x for the samples heat-treated under different conditions. The images show the presence of very fine and homogeneously distributed grains. Also, some larger grains and different morphologies can be observed, which are dispersed. It is also possible to observe porosity in the samples. The formation of the fine-grained microstructure is attributed to the processing method (powder metallurgy), as the initial powders, with a particle size of ~5 μm, were further reduced during the milling stage to ~2.82 μm. Undoubtedly, during sintering, grain growth occurs; however, as can be observed in this figure, it was not excessive. Another important factor to consider is the presence of silver, which some researchers have identified as a grain refiner.[22–24]

To enable a more detailed observation of the microstructural characteristics, the samples were analyzed using a scanning electron microscope. Fig. 4 shows the phases comprising the microstructure, represented by different shades of gray. Particles ranging from 3 to 5 microns in size are observed to be dispersed throughout the alloy matrix. The darker regions correspond to grain boundaries within the microstructure. Also, porosity formation is evident, although the overall porosity is minimal.

Fig. 4, *d* corresponds to a micrograph taken using the backscattered electron technique. This image clearly shows the formation of precipitates in intragranular zones, which were identified as regions of higher contrast due to their differences in chemical composition, of very small size, and uniform dispersion within the surrounding matrix. This image indicates that precipitate formation occurred during the thermal aging treatment.

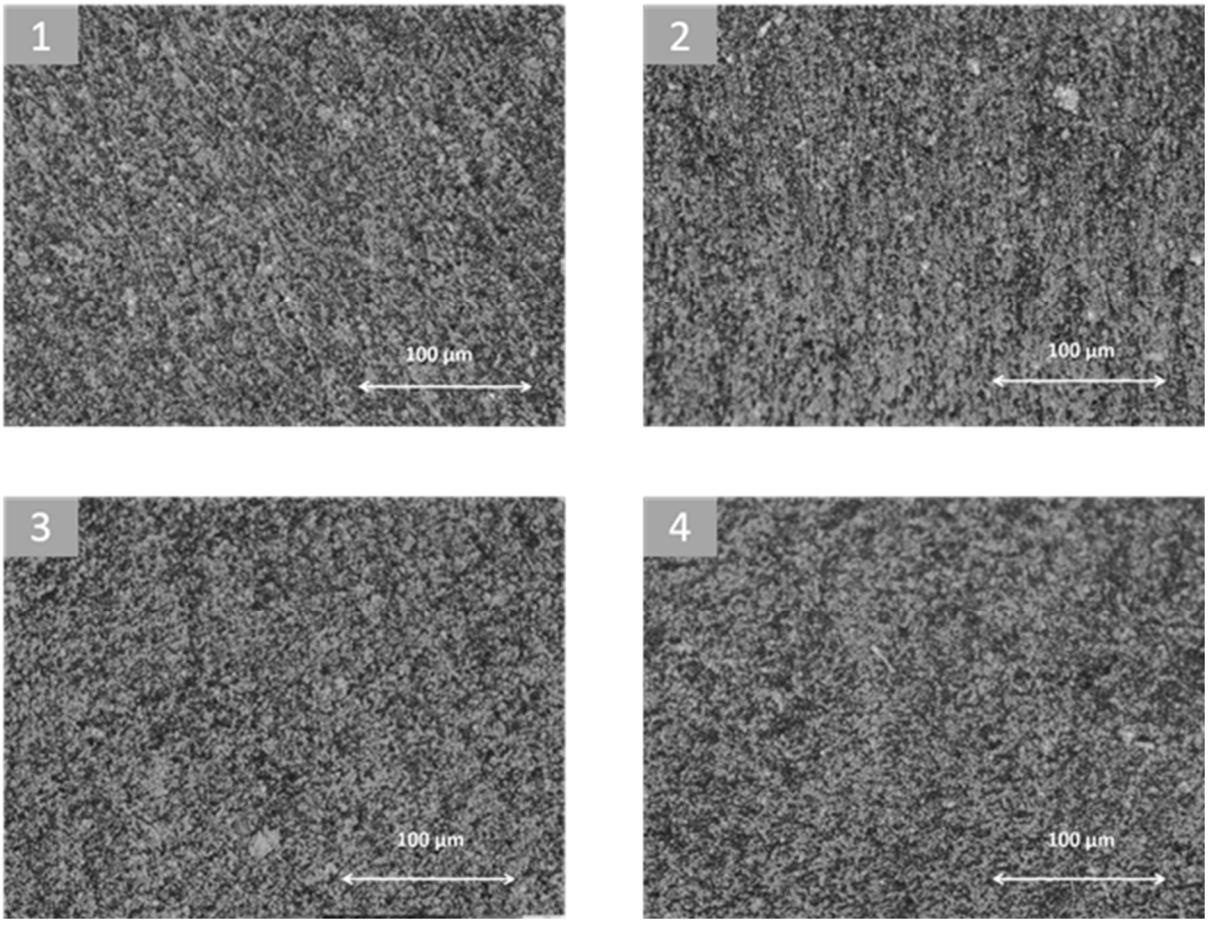

Fig. 3. Micrographs of the AlCuAg alloy surface of each sample

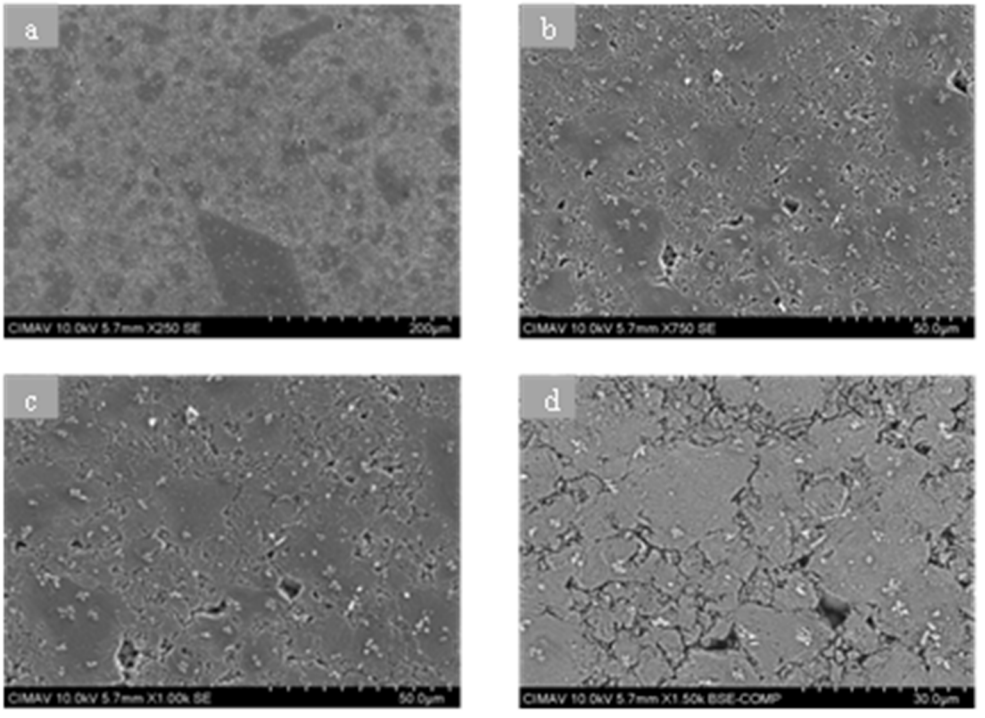

Fig. 4. SEM micrographs of the different sintered and aged samples

3.4. EDS analysis

Fig. 5 shows an enlarged image of the sample representing the matrix with the presence of some precipitates. In this image, chemical analyses were carried out in different areas to determine the elements present. The image (left side) shows the area where the analysis was performed, and the right side shows the result for each spectrum performed. Spectra 14, 15, and 16 correspond to particles where a higher amount of copper is concentrated, in a ratio of 17 to 25 % by weight, while for spectra 17, 18, and 19, corresponding to the matrix of the alloy, the amounts of Cu and Ag remain close to the nominal composition of 1.5 % with a deviation ± 0.5. On the other hand, oxygen is observed in all the spectra, likely due to the alloy's chemical reaction with atmospheric oxygen during the sintering stage.

Fig. 6 shows a mapping of the image in Fig. 5, where different shades indicate the locations of each element. Green highlights areas with a higher oxygen concentration, primarily near the grain boundaries. Copper is concentrated in the orange areas corresponding to the precipitates, while silver is evenly distributed within the aluminum matrix, represented by the purple areas.

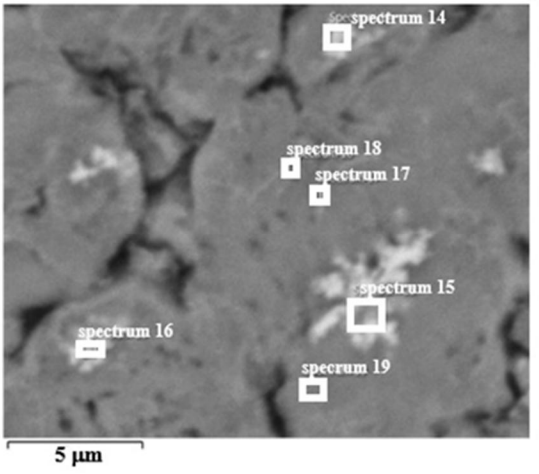

Spectrum 14	Wt. %	σ
Al	72.5	0.4
Cu	17.0	0.4
O	9.0	0.2
Ag	1.5	0.1

Spectrum 15	Wt. %	σ
Al	68.0	0.4
Cu	25.4	0.5
O	5.1	0.1
Ag	1.5	0.2

Spectrum 16	Wt. %	σ
Al	70.3	0.4
Cu	20.1	0.4
O	8.1	0.2
Ag	1.3	0.2

Spectrum 17	Wt. %	σ
Al	80.5	0.3
Cu	0.9	0.2
O	16.9	0.2
Ag	1.7	0.2

Spectrum 18	Wt. %	σ
Al	81.2	0.3
Cu	1.2	0.3
O	16.0	0.2
Ag	1.6	0.2

Spectrum 19	Wt. %	σ
Al	90.4	0.3
Cu	1.1	0.3
O	6.5	0.2
Ag	2.0	0.2

Fig. 5. Elemental chemical analysis of different spectra in the AlCuAg alloy

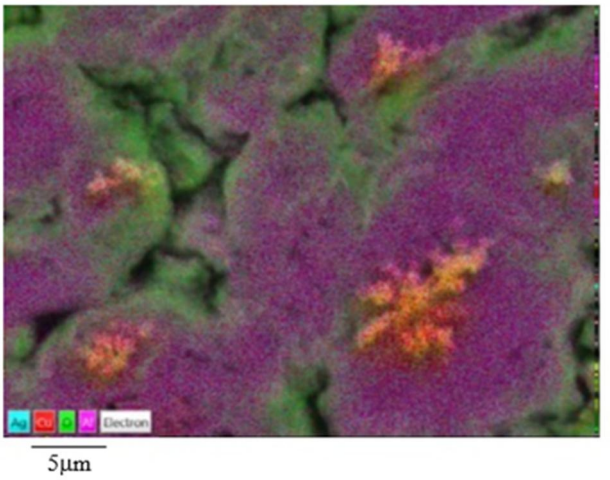

Fig. 6. Mapping of the area containing some precipitates, obtained by EDS

Fig. 7 shows a line scan performed with EDS in the area of the precipitates. An increased concentration of copper is observed within the grains, whereas the silver content remained constant. On the other hand, a slight increase in oxygen is also observed. These findings confirm that the precipitate location is transgranular. Based on the observed results, it can be concluded that the alloy is constituted by two phases: the α-phase, corresponding to the aluminum matrix, and the β–phase, associated with intermetallic compounds of the copper-rich AlCuAg alloy.

Fig. 8 shows a mapping of the alloy, indicating the presence and distribution of its components. As can be seen, silver is homogeneously distributed throughout the matrix. The presence of copper in the matrix is clear, but it is mainly concentrated in the precipitates. Additionally, aluminum is observed in the matrix, with a certain degree of oxidation.

3.5. Mechanical properties

3.5.1 Microhardness

To evaluate the alloy's mechanical properties, Vickers microhardness testing was initially conducted. Fig. 9 shows the hardness values of 9 typical high-entropy systems as well as those of a commercial alloy, compared to the values achieved in samples treated by thermal aging of the medium-entropy AlCuAg system. As can be seen in this table, the hardness achieved by the medium-entropy AlCuAg alloy manufactured here exceeds that of the different high-entropy alloys and even those of commercial alloys. This result is due to the formation of copper-rich precipitates in the alloy during the aging treatments. On the other hand, with respect to the treatments applied, it was found that longer exposure times influenced a greater hardness of the alloy. Likewise, the higher treatment temperature resulted in a greater formation and distribution of copper precipitates, which is reflected in higher hardness values.

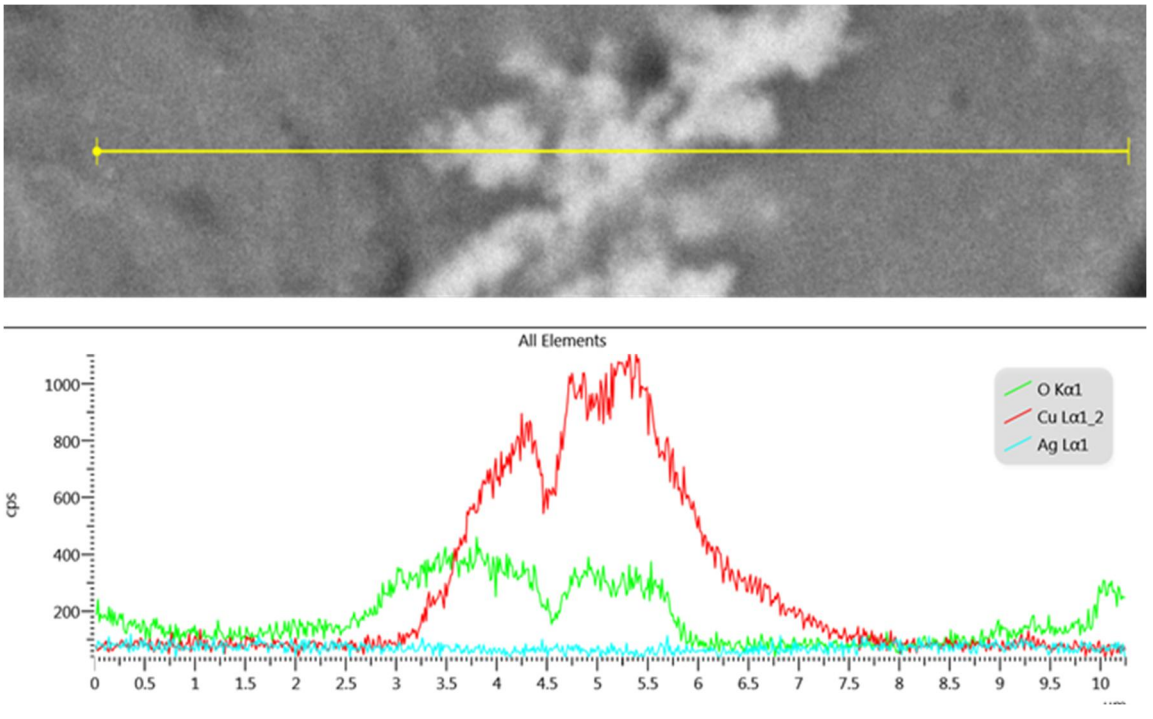

Fig. 7. Line scanning by energy dispersive X-ray spectroscopy to determine the elements present in the precipitates

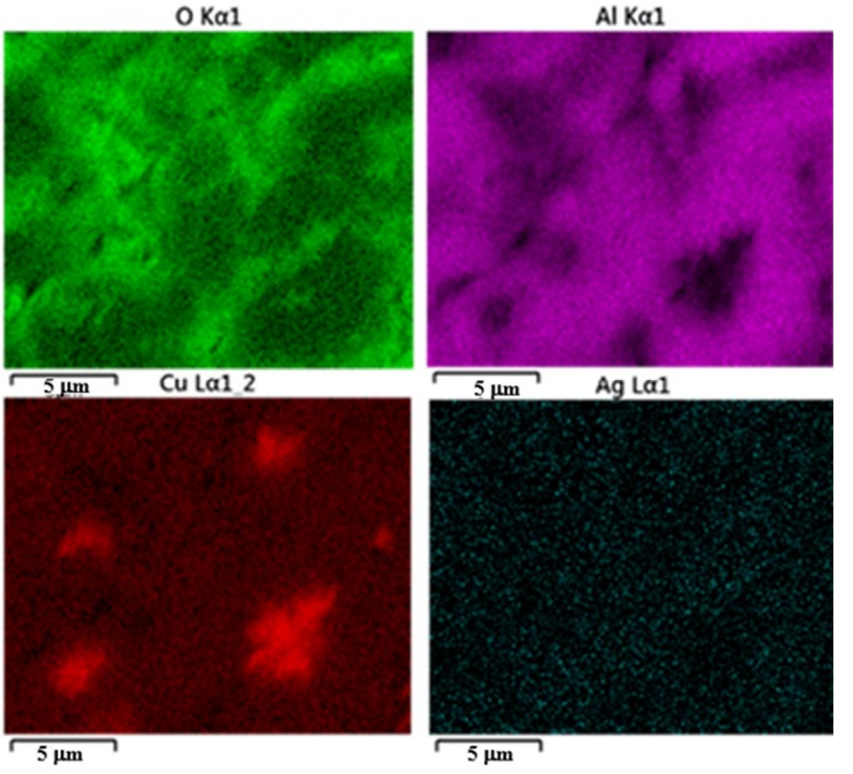

Fig. 8. EDS mapping to observe element distribution in the AlCuAg alloy

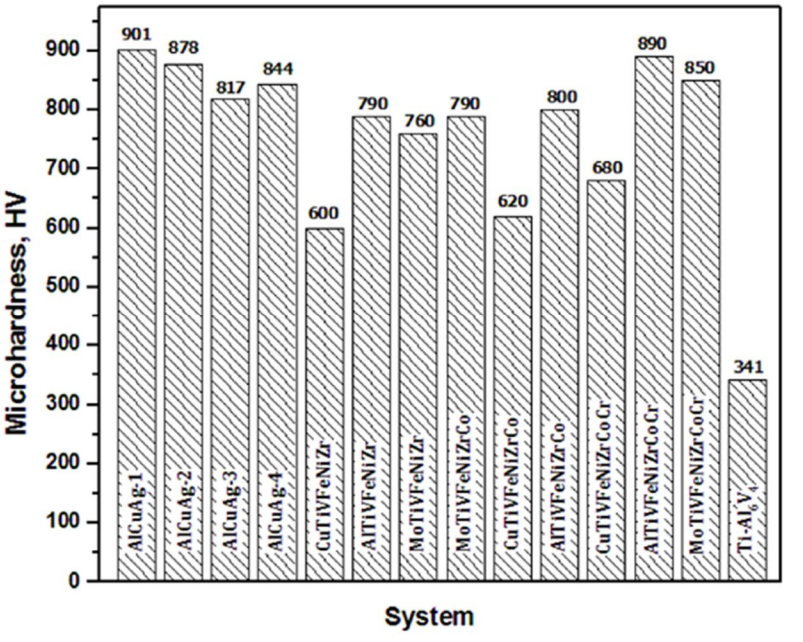

Fig. 9. Comparison between the hardness of the alloys processed here and different HEA

3.5.2. Compression test

Fig. 10 shows a comparison of the stress-strain curves of the sample's compression test. The curves show similar material behavior in each of the samples. However, sample 1 stands out remarkably in one property, achieving the highest compressive strength with a maximum stress value of 2051 MPa. This result corresponds to the thermal

aging treatment at a lower temperature but with longer exposure time, *i. e*., 300 °C for 5 h. This outcome aligns with the highest hardness values obtained in the previous tests, as well as the Young's modulus test conducted using the ultrasound technique. Table 2 shows some of the most representative mechanical properties obtained from the analysis of the stress-strain curves.

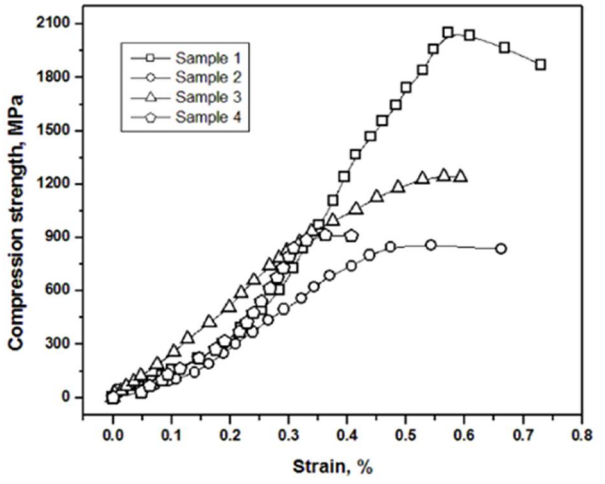

Fig. 10. Stress-strain curves of the sample's compression test

Table 2. Main mechanical properties of samples obtained from the compression test

Property	S1	S2	S3	S4
Elastic modulus, GPa	154	98	252	172
Maximum stress, MPa	2051	859	1246	916
Yiel stress, MPa	301	143	505	314
Fracture stress, MPa	1870	835	1237	908

4. Conclusions

In this research, a medium-entropy alloy composed of aluminum with equiatomic amounts of copper and silver was synthesized by the powder processing route and subjected to different aging treatments. Several characterization studies were conducted using techniques such as X-Ray Diffraction (XRD), Scanning Electron Microscopy (SEM), and Optical Microscopy (OM). This study allowed us to describe the microstructural characteristics of the system, as well as its relationship with the synthesis process and its final mechanical properties of hardness and compressive strength, obtaining the following conclusions:

- Through the mechanical milling process carried out for 6 hours at 300 rpm, the average particle size of the alloy was reduced to less than 3 microns, achieving a significant refinement of the material.
- Based on the results of EDS analysis, a fine microstructure consisting of two phases was observed: an α matrix of near-nominal AlCuAg composition and an intermetallic β phase with dispersed copper-rich AlCuAg particles. On the other hand, Ag atoms were homogeneously dissolved in both phases, ensuring a uniform distribution in the solution.
- The medium entropy AlCuAg alloy heat-treated at 300 °C for 5 h showed higher mechanical strength in compression, as well as superior Young's modulus and microhardness values, compared to its variants treated at 350 °C for 2 h. This result indicates that the precipitation hardening mechanisms were more effective at lower temperatures with longer residence times.
- The increase in the mechanical properties of the alloy can be attributed to increased atomic disorder, generated by the elevated entropy in the matrix-strengthening solid solution, as well as to the formation of precipitates during aging treatments that act as obstacles to the movement of dislocations.

Acknowledgements

A. A. C. M. would like to express the appreciation to CONAHCyT for the grant to carry out her master's degree studies.

References

[1] Rambabu, P.; Eswara P. N.; Kutumbarao, V. V.; Wanhill, R. J. H. Aluminium Alloys for Aerospace Applications, in Aerospace Materials and Material Technologies: Aerospace Materials, Prasad N. E. and Wanhill, R. J. H. Eds.; Springer Singapore: Singapore, 2017; pp. 29–52.
[2] *ASM Handbook, Properties and Selection: Nonferrous Alloys and Special-Purpose Materials*; ASM International, USA, 1992; pp. 2–60.
[3] Du, X.; Ma, X.; Ding, X.; Zhang, W.; He, Y. Enhanced High-Temperature Oxidation Resistance of Low-Cost Fe–Cr–Ni Medium Entropy Alloy by Ce-Adulterated. *J. Mater. Res. Technol*. **2022**, *16*, 1466–1477. https://doi.org/10.1016/j.jmrt.2021.12.087
[4] Doty, H. W.; El-Hadad, S.; Samuel, E.; Samuel, A. M.; Samuel, F. H. The Influence of Rare Earth Metals on the Microstructure and Mechanical Properties of 220 and 356.1 Alloys for Automotive Industry. *Materials* **2025**, *18*, 941. https://doi.org/10.3390/ma18050941
[5] Yeh, J.-W. High-Entropy Alloys: Overview. *Encyclopedia of Materials: Metals and Alloys* **2022**, *2*, 294–307. https://doi.org/10.1016/B978-0-12-819726-4.00130-7
[6] Mohammed, A. B.; Abdul, J. New Solid-Solutions of Substitution Strontium (Sr) for Lead (Pb) in Apatite Structure. *Chem. Chem. Technol*. **2023**, *17*, 719–728. https://doi.org/10.23939/chcht17.04.719
[7] Cantor, B. Multicomponent and High Entropy Alloys. *Entropy* **2014**, *16*, 4749–4768. https://doi.org/10.3390/e16094749

[8] He, H.; Wang, Y.; Qi, Y.; Xu, Z.; Li, Y. Review on the Preparation Methods and Strengthening Mechanisms of Medium-Entropy Alloys with CoCrNi as the Main Focus. *J. Mater. Res. Technol.* **2023**, *27*, 6275–6307. https://doi.org/10.1016/j.jmrt.2023.10.266
[9] Wu, X. Chemical Short-Range Orders in High-/Medium-Entropy Alloys. *J. Mater. Res. Technol*. **2023**, *147*, 189–196. https://doi.org/10.1016/j.jmst.2022.10.070
[10] Lv, J.; Yu, H.; Fang, W.; Yin, F.; Wei, D. Manipulation of Precipitation and Mechanical Properties of Precipitation-Strengthened Medium-Entropy Alloy. *Scr. Mater.* **2023**, *222*, 115057. https://doi.org/10.1016/j.scriptamat.2022.115057
[11] Han, Z.; Meng, L.; Yang, J.; Liu, G.; Yang, J.; Wei, R.; Zhang, G. Novel BCC VNbTa Refractory Multi-Element Alloys with Superior Tensile Properties. *Mater. Sci. Eng., A* **2021**, *825*, 141908. https://doi.org/10.1016/j.msea.2021.141908
[12] Behzad, Z.; Masumeh, G. The Immobilized Cu-Ni-Fe-Cr Layered Double Hydroxide on Silica-Layered Magnetite as a Reusable Mesoporous Catalyst for Convenient Conversion of Epoxides to 1,2-Diacetates. *Chem. Chem. Technol*. **2023**, *17*, 279–286. https://doi.org/10.23939/chcht17.02.279
[13] Do, H.-S.; Moon, J.; Kim, H. S.; Lee, B.-J. A Thermodynamic Description of the Al–Cu–Fe–Mn System for an Immiscible Medium-Entropy Alloy Design. *Calphad.* **2020**, *71*, 101995. https://doi.org/10.1016/j.calphad.2020.101995
[14] Yeh J.-W.; Chen, S.-K.; Lin, S.-J.; Gan, J.-Y.; Chin, T.-S.; Shun, T.-T.; Tsau, C.-H.; Chang, S.-Y. Nanostructured High-Entropy Alloys with Multiple Principal Elements: Novel Alloy Design Concepts and Outcomes. *Adv. Eng. Mater.* **2004**, *6*, 299–303. https://doi.org/10.1002/adem.200300567
[15] Qiu, S.; Zheng, G. P.; Jiao, Z. B. Alloying Effects on Phase Stability, Mechanical Properties, and Deformation Behavior of CoCrNi-Based Medium-Entropy Alloys at Low Temperatures. *Intermetallics.* **2022**, *140*, 107399. https://doi.org/10.1016/j.intermet.2021.107399
[16] Huang, Y.; Yu, X.; Deng, L.; Gao, Y.; Wang, S.; Wang, B. Microstructure and Mechanical Properties of the (TiZrV)100-xAlx Medium-Entropy Alloys. *J. Mater. Res. Technol*. **2023**, *23*, 2824–2835. https://doi.org/10.1016/j.jmrt.2023.01.192
[17] Dingfeng, X.; Mingliang, W.; Tianxin, L.; Xiangsai, W.; Yiping, L. A Critical Review of the Mechanical Properties of CoCrNi-Based Medium-Entropy Alloys. *Microstructures.* **2022**, *2*, 2022001. http://dx.doi.org/10.20517/microstructures.2021.10
[18] Wu, X. L.; Zhu, H. A Non-Equiatomic Ni-Co-Fe Medium-Entropy Alloy with Excellent Wear Resistance and Strength-Ductility Combination by Adding Al. *Mater. Charact.* **2023**, *205*, 113305. https://doi.org/10.1016/j.matchar.2023.113305
[19] Yujing, Y. J. Y.; Dong, Y.; Liu, S.; Li, C.; Zhang, P.; Duan, S. Microstructure, Mechanical and Corrosion Properties of Al–Co–Cr–Ni Near Eutectic Medium Entropy Alloys. *J. Mater. Res. Technol.* **2024**, *29*, 5149–5160. https://doi.org/10.1016/j.jmrt.2024.03.014
[20] Li, J.; Xie, B.; Fang, Q.; Liu, B.; Liu, Y.; Liaw, P. K. High-Throughput Simulation Combined Machine Learning Search for Optimum Elemental Composition in Medium Entropy Alloy. *J. Mater. Sci. Technol*. **2021**, *68*, 70–75. https://doi.org/10.1016/j.jmst.2020.08.008
[21] ASTM E384 – 16, Standard Test Method for Microindentation Hardness of Materials, last update 2017.
[22] Babacan, N.; Kochta, F.; Hoffmann, V.; Gemming, T.; Kühn, U.; Giebeler, L.; Gebert, A.; Hufenbach, J. Effect of Silver Additions on the Microstructure, Mechanical Properties and Corrosion Behavior of Biodegradable Fe-30Mn-6Si. *Mater. Today Commun.* **2021**, *28*, 102689. https://doi.org/10.1016/j.mtcomm.2021.102689
[23] Zhao, X.; Zheng, H.; Ma, X.; Sheng, Y.; Zeng, D.; Yuan, J. Microstructure, Mechanical Properties and Corrosion Resistance of Ag-Cu Alloys with La_2O_3 Fabricated by Selective Laser Melting. *Materials.* **2023**, *16*, 7670. https://doi.org/10.3390/ma16247670
[24] Shakouri, M.; Esmailian, M.; Shabestari, S. Effect of Silver Addition on Mechanical Properties and Stress Corrosion Cracking in a Predeformed and Overaged 7055 Aluminum Alloy. *J. Test. Eval.* **2018**, *46*, 1891–1900. https://doi.org/10.1520/JTE20170137

Received: April 26, 2025 / Revised: July 03, 2025 / Accepted: September 03, 2025

МЕХАНІЧНА ТА МІКРОСТРУКТУРНА ХАРАКТЕРИСТИКИ ALCuAg СПЛАВУ

Анотація. *Алюмінієві сплави широко використовують в автомобільній та авіаційній промисловості завдяки хорошим механічним властивостям, високій корозійній стійкості та невеликій вазі. Для дослідження було виготовлено алюмінієвий сплав середньої ентропії із додаванням міді та срібла. Сплав складався з 97 % алюмінію, 1,5 % міді та 1,5 % срібла. Технологію оброблення було реалізовано за допомогою порошкової металургії. Після фази спікання здійснено різні термічні оброблення за неоднакових тривалостей і температур для поліпшення механічних властивостей алюмінієвого сплаву. У результаті виявлено мікроструктуру з дуже дрібним розміром зерен, що складається з двох фаз: матриці α-твердого розчину зі складом, близьким до номінального сплаву, та інтерметалічної β-фази, що складається з дисперсних, багатих на мідь осадів AlCuAg.*

Ключові слова: *сплави, багатокомпонентні, сплави середньої ентропії, AlCuAg.*